Graph Neural Networks for Photon Searches with the Underground Muon Detector of the Pierre Auger Observatory

Ezequiel Rodriguez[ab,*] **on behalf of the Pierre Auger Collaboration**[c]

[a]*Instituto de Tecnologías en Detección y Astropartículas (CNEA, CONICET, UNSAM), Av. General Paz 1555 (B1630KNA) San Martín, Buenos Aires, Argentina*

[b]*Institute for Astroparticle Physics (IAP), Karlsruhe Institute of Technology, P.O. Box 3640, 76021 Karlsruhe, Germany*

[c]*Observatorio Pierre Auger, Av. San Martín Norte 304, 5613 Malargüe, Argentina*
Full author list: https://www.auger.org/archive/authors_icrc_2025.html

E-mail: spokespersons@auger.org

Ultra-high-energy photons have long been sought as tracers of the most energetic processes in the Universe. Several sources can contribute to a diffuse photon flux, including interactions of cosmic rays with Galactic matter and radiation fields, as well as more exotic scenarios such as the decay of super-heavy dark matter. Regardless of their origin, the expected flux is extremely low, making direct detection impractical and thereby requiring indirect detection by extensive ground-based detector arrays. In this contribution, we present a novel method for photon–hadron discrimination in the energy range of 50 to 300 PeV based on deep learning algorithms. Our approach relies on information from both the Surface Detector (SD) and the Underground Muon Detector (UMD) of the Pierre Auger Observatory. The SD consists of an array of water-Cherenkov detectors. It is used to measure the electromagnetic and muonic components of extensive air showers at ground level. Meanwhile, the UMD is composed of buried scintillator modules. It is sensitive to air-shower muons with energies above ~1 GeV, enhancing the identification of muon-poor air showers as initiated by photon primaries. Our method represents air-shower events as graphs, and consequently, the network architecture is composed of graph attention layers. We assess the performance of the method on a data subset and discuss the implications of unblinding the full current dataset, as well as the prospects of the increasing data volume expected in the coming years, particularly in terms of sensitivity to various diffuse fluxes from theoretical predictions.

ICRC 2025
The Astroparticle Physics Conference
Geneva July 15-24, 2025

---
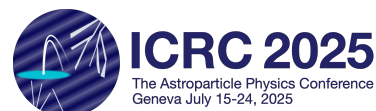
[*]Speaker

1. Introduction

Ultra-high-energy (UHE) photons serve as valuable tracers of the most energetic phenomena in the Universe. The detection of UHE photons gives insights into cosmic-ray interactions with matter and radiation fields, such as those in the Galactic plane or nearby extragalactic environments, as well as into more exotic scenarios like the decay of super-heavy dark matter (SHDM) particles [1–4]. UHE photon fluxes at Earth are expected to originate primarily from the Milky Way and its satellite galaxies. More distant sources are strongly attenuated, as photon interaction lengths are on the order of 0.1 Mpc. Despite the rich physics potential, the diffuse photon flux is expected to lie several orders of magnitude below the flux of charged cosmic rays, making direct detection unfeasible. As an alternative approach, large surface detector arrays enable indirect detection by measuring secondary particles from extensive air showers (EAS). In particular, photon-induced showers develop deeper in the atmosphere and produce significantly fewer muons than hadron-initiated showers.

The Pierre Auger Observatory is based on a multi-hybrid design, aimed to study ultra-high-energy cosmic rays using complementary detection techniques. The Surface Detector (SD) comprises an array of water-Cherenkov detectors (WCDs) arranged in triangular grids at 1500, 750, and 433 m spacings, and measures the electromagnetic, the hadronic, and the muonic components of the EAS. To improve its sensitivity to the different air-shower components, which in turn would provide valuable information toward the discrimination of photon primaries in the cosmic-ray background, the final phase of the AugerPrime upgrade is currently undergoing [5]. This includes the installation of the Underground Muon Detector (UMD) [6, 7], composed of buried scintillator modules located next to WCDs in the SD-750 and SD-433. These stations are shielded by 2.3 m of soil to suppress the electromagnetic component [8, 9] and measure air-shower muons with $\gtrsim 1$ GeV. Muons penetrating the soil produce light in the scintillator bars, which is read out by silicon photomultipliers (SiPMs).

In this work, we propose a novel method for photon–hadron discrimination in the energy range from 50 to 300 PeV using Graph Neural Networks (GNNs). By representing air showers as graphs, we leverage GNNs to process the geometric detector layout and integrate input features from both the SD-433 and UMD. The model architecture is built from graph attention layers, which naturally account for any irregularity in the detector grid. After training and evaluating our method with simulated air-shower events, we apply it to a subset of data used in previous photon search studies [10], confirming its future application in larger datasets.

2. Simulations

Extensive air showers were generated with CORSIKA [11] using the hadronic interaction model EPOS LHC [12]. The detector responses of the SD-433 and the UMD were modeled with the AugerOffline framework [13]. Primary particles were sampled isotropically, with uniform distributions in $\sin^2 \theta_{MC}$ and azimuthal angle ϕ_{MC}, and energies spanning the range $\lg(E_{MC}/eV) \in$ [16.0, 17.5]. The simulation includes the arrival of secondary particles at the SD stations and the propagation of muons through 2.3 m of soil to the UMD, along with the associated optoelectronics response and signal acquisition for each detector.

A preliminary set of photon simulations was used for two purposes: first, to estimate the array photon detection efficiency as a function of the primary energy and zenith angle; and second, to

optimize the event reconstruction for photon-initiated showers.

The main set of simulated events was divided into training, validation, and testing data sets. All events in these sets verify a minimum efficiency of 0.9. The training data set includes ∼160, 000 simulated events, equally divided between photon- and proton-induced showers. The validation data set contains ∼40, 000 events with the same composition. The test data set comprises approximately ∼60, 000 photon and proton events, and an additional ∼50, 000 iron-induced showers, allowing assessment of the model's response to a broader range of primary masses.

3. Event reconstruction

To quantify the performance of the SD-433 array in detecting photon-induced air showers, we estimated the reconstruction efficiency by fitting a probit model to the photon simulations using a binomial likelihood. The efficiency $\varepsilon(E_{MC}, \theta)$ quantifies the probability that a photon primary with energy E_{MC} and zenith angle θ_{MC} is successfully reconstructed. In this work, the analysis is restricted to events with $\lg(E_{MC}/eV) \geq 16.7$, corresponding to a phase space where photon–hadron discrimination is currently acceptable. The zenith angle is indirectly restricted by the efficiency requirement. The resulting efficiency curves (see Fig. 1) reveal that the SD-433 array remains efficient down to lower energies for vertical showers. This demonstrates the potential for extending photon searches to lower energy regimes in the future, as long as separation remains feasible.

Figure 1: Estimated reconstruction efficiency, ε, for photon-induced showers as a function of $\lg(E_{MC}/eV)$ and $\sin^2 \theta_{MC}$. Contours for 99% and 90% efficiency are shown in yellow and orange, respectively.

To ensure a consistent energy scale for all primary particles, all events in this study were reconstructed using photon priors. To reconstruct the *photon energy* E_γ of a primary, we adopt a dedicated Monte Carlo calibration based on the lateral distribution function (LDF) of the SD signals, similar to [10]. The energy estimate is based on the expected signal $S(300)$ at 300 m from the shower axis, selected as the reference distance for the SD-433 due to its optimal balance between resolution and systematics [14].

It is important to note that the reconstruction procedure assumes the photon hypothesis: the LDF and the inferred energy correspond to the expectation for photon-induced showers. When applied to hadronic primaries, such as protons or iron nuclei, this introduces a bias due to their higher muon content and distinct development. In other words, the approximation $E_{MC} \sim E_\gamma$ holds only for photon events. As a result, both the efficiency estimation and the reconstructed energy of hadronic events (in data or simulations) will be systematically biased, since selection cuts are based on signal observables calibrated for photons. Nevertheless, this does not affect the classification performance, as the deep learning model developed in this work does not use the reconstructed
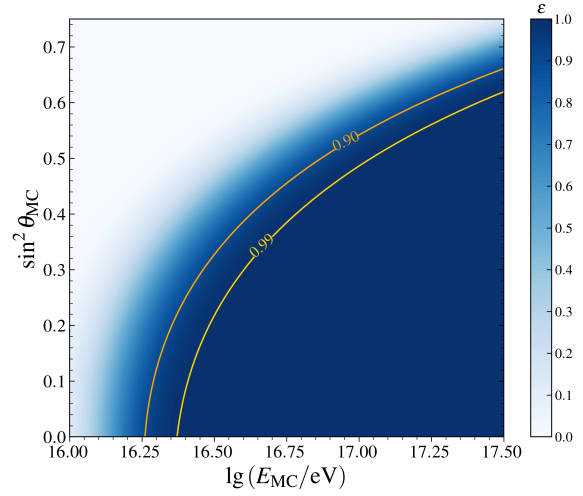
energy as an input feature. The use of a photon energy scale, E_γ, thus provides a consistent reference for comparing and analyzing all primary types in a photon search.

The energy estimator is defined by

$$\frac{S(300)}{g(\theta)} = \left(\frac{E_{\mathrm{MC}}}{100 \text{ PeV}}\right)^{\alpha(\theta)}, \tag{1}$$

where the power is a third-degree polynomial

$$\alpha(\theta) = \alpha_0 + \alpha_1(\cos^2\theta) + \alpha_2(\cos^2\theta)^2 + \alpha_3(\cos^2\theta)^3, \tag{2}$$

and the attenuation function takes the form of a Gaisser-Hillas curve

$$g(\theta) = g_0\left(1 + \frac{x - g_2}{g_1}\right)^{g_1/g_3}\exp\left(-\frac{x - g_2}{g_3}\right), \quad \text{with } x = \sec\theta - \sec 25°. \tag{3}$$

Calibration is performed using simulated photon showers that pass an efficiency cut of $\varepsilon >$ 0.9. The resulting energy estimator is unbiased to within ∼1% across the interval $\lg(E_{\mathrm{MC}}/\mathrm{eV}) \in$ [16.4, 17.5], with an energy resolution of ∼14% for zenith angles up to 45°. In the range between 45° and 55°, the bias can increase up to ∼5%, and the resolution degrades to ∼30%. The attenuation function $g(\theta)$ is characterized by best-fit parameters $g_0 = 23.04 \pm 0.06$, $g_1 = 0.249 \pm 0.014$, $g_2 = -0.076 \pm 0.003$, and $g_3 = 0.165 \pm 0.004$. The exponent $\alpha(\theta)$ is modeled as a cubic polynomial in $\cos^2\theta$, with coefficients $\alpha_0 = 1.96 \pm 0.09$, $\alpha_1 = -4.49 \pm 0.22$, $\alpha_2 = 6.06 \pm 0.09$, and $\alpha_3 = -2.49 \pm 0.06$.

4. Graph representation and model architecture

An earlier version of the neural network used in this work was presented in [15], where a dual-graph representation was used to separately encode information from the SD and the combined SD–UMD event. In the current implementation, we adopt a refined design that reduces memory usage, avoids redundancy, and allows for more flexible input handling, while retaining the original concept of separating and analyzing the contributions from the SD, UMD, and their joint information.

Each event is represented as a single undirected graph $\mathcal{G} = (\mathcal{V}, \mathcal{E})$, where the set of nodes $\mathcal{V}$ correspond to triggered SD stations connected by a set of edges $\mathcal{E}$. The graph is described by three matrices: the adjacency matrix $A \in \mathbb{R}^{N \times N}$, where $A_{ij} = 1$ if stations i and j are connected (up to second neighbors in the 433 m triangular grid); the feature matrix $X \in \mathbb{R}^{N \times F}$, containing for each node spatial and temporal offsets relative to the station with the largest signal, number of working photomultiplier tubes (PMTs) in each WCD, WCD measured signal, muon density ρ_μ, and UMD effective area[1]; and the trace matrix $X_{\mathrm{traces}} \in \mathbb{R}^{N \times T}$, consisting of the first 60 time bins (25 ns each) of the averaged SD trace over available PMTs.

Due to data augmentation in simulations or the presence of non-operational UMD stations in data, some nodes may have missing values in UMD-related features. These are handled using

---

[1]The effective area represents the projected area of the UMD modules in the shower front, accounting for the orientation and geometric alignment of the modules relative to the incoming air shower. The muon density ρ_μ is the estimated number of muons divided by such area.
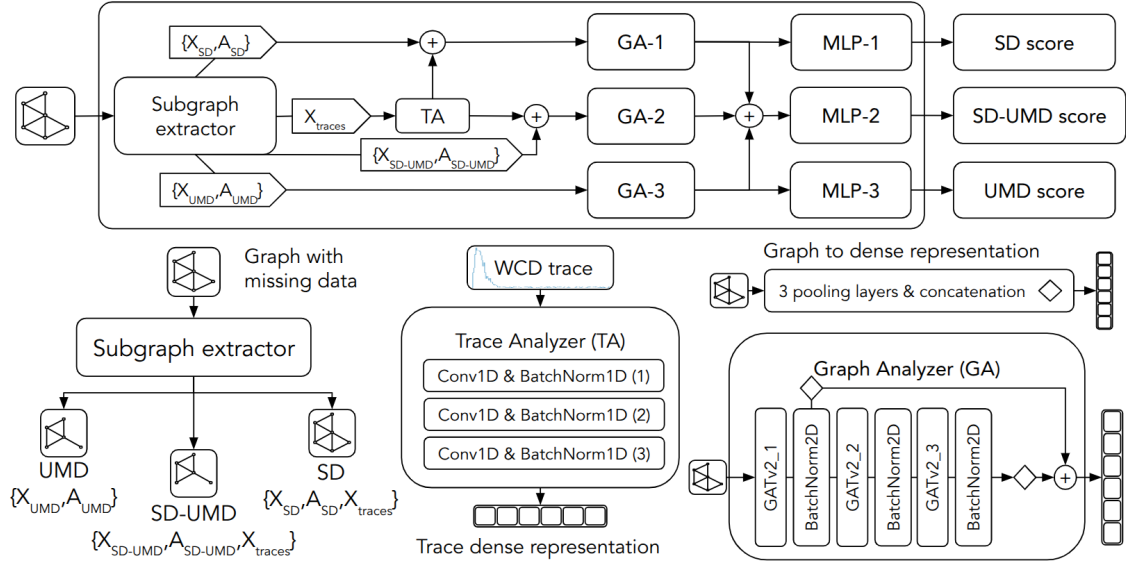
4

Figure 2: Schematic of the updated neural network architecture and its modular subcomponents. A single graph encodes SD and UMD information. Binary masks guide the Subgraph Extractor in generating SD, UMD, and SD–UMD subgraphs. Trace features are computed and added to the relevant nodes before graph attention layers (GATv2) are applied. Global pooling operations (mean, max, and sum) are performed on the first and third GATv2 outputs, and their concatenation is passed to MLPs to obtain photon-like scores.

precomputed binary masks indicating the validity of each detector component at every station. A dedicated subcomponent, the *Subgraph Extractor*, uses these masks to dynamically isolate the SD-only, UMD-only, and joint SD–UMD subgraphs during training and inference. This approach eliminates the need to store redundant graph copies and significantly reduces memory consumption per event compared to the earlier design [15].

Fig. 2 shows a sketch of the improved architecture. The *Trace Analyzer* (TA), unchanged from the previous network version, processes SD time traces using 1D convolutional layers, producing features concatenated with the node attributes for SD and SD–UMD processing. The node features are processed through three distinct *Graph Analyzers* (GA) corresponding to SD, UMD, and SD–UMD. Each GA consists of three GATv2 layers [16]. In the updated network, pooling operations (mean, max, sum) are applied to both the first and third outputs of the GATv2 layers, and the results are concatenated before being passed to the classification multi-layer perceptrons (MLPs). This enriches the final graph embedding by combining low- and high-level representations. Each of the three graph-level embeddings is then processed by a dedicated MLP to produce a photon-like classification score.

Unlike the earlier joint training strategy, the network is currently trained using a sequential and independent path optimization approach: the UMD path is trained first; all other weights, including the Trace Analyzer, other GATv2 layers, and MLPs, are kept frozen; next, the SD path is trained, with its corresponding GATv2 and MLP, as well as the shared Trace Analyzer, being updated while the rest of the network remains fixed; finally, the SD–UMD path is trained using its dedicated GATv2 and MLP, keeping all previously trained components frozen.

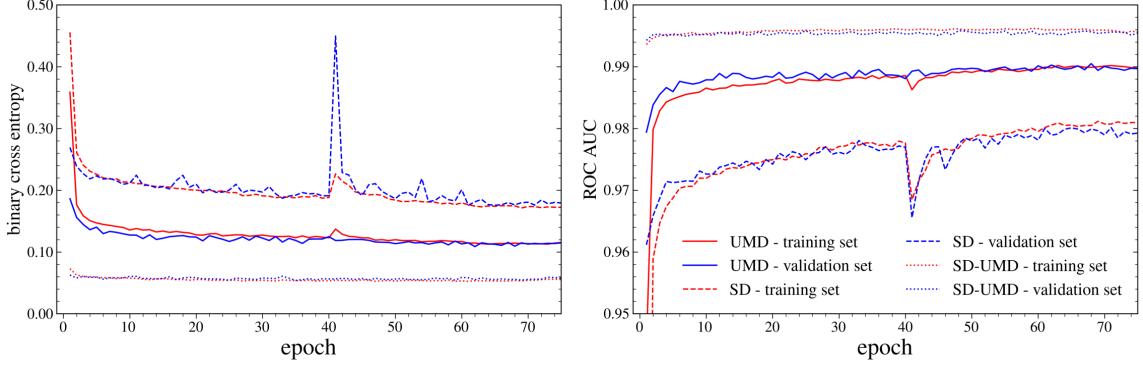This training strategy allows each head to specialize in extracting the most informative fea-

Figure 3: Training and validation performance for each path. Left panel: binary cross-entropy loss. Right panel: ROC-AUC scores. The close match between training and validation curves indicates stable generalization.

tures from its respective data stream, while avoiding inter-path interference. Each sub-network is optimized using the binary cross-entropy loss between its photon-like score and the true event label.

As shown in Fig. 3, the training curves for each information path remain closely aligned with their respective validation metrics, indicating no significant overfitting. Among the three outputs, the SD–UMD path consistently exhibits the highest performance. Notably, the UMD-only path also provides strong discrimination, reflecting the value of direct muon measurements in photon searches.

5. Photon-hadron discrimination

The trained deep learning model provides effective separation between photon and hadron primaries, with the SD–UMD score consistently outperforming the UMD-only and SD-only classifiers. This ordering in discrimination power is already observed in the training and validation curves (see Fig. 3).

To quantify background contamination, we focus on the SD–UMD score as the most powerful discriminator. Figure 4 shows the estimated background contamination as a function of signal efficiency in four energy bins. Contamination was computed by modeling the score distribution of the most photon-like proton events using exponential fits to the tail region. Due to the limited number of events in the tails, a bootstrapping procedure was employed to esti-

Figure 4: Estimated background contamination vs. signal efficiency in four energy intervals. Shaded bands correspond to bootstrap uncertainties on the exponential tail fits used to model the background score distributions.

mate the uncertainty on the slope. Small variations in the slope significantly affect the background contamination expectation at high rejection levels.
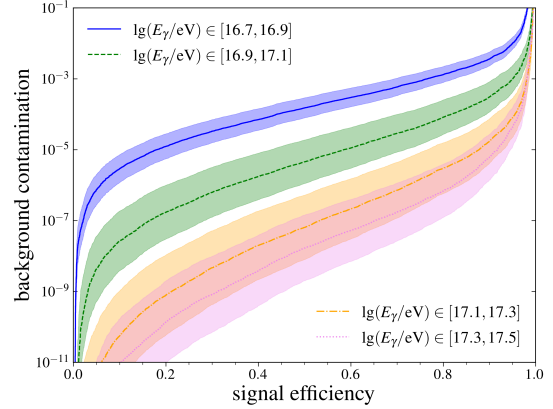
6

At a fixed signal efficiency of 0.5, the average background contamination in the bins $\lg(E_\gamma/\text{eV}) \in$ [16.7, 16.9), [16.9, 17.1), [17.1, 17.3), and [17.3, 17.5) is below 8×10^{-5}, 10^{-5}, 10^{-7}, and 10^{-8}, respectively. It is worth noting that these estimates include the effect of random PMT and UMD module masking, as well as entire SD or UMD station removal, to emulate real operation conditions. As such, they represent conservative values compared to idealized simulations.

To validate the applicability of the model to experimental data, we use a subset of events that were previously burnt in a photon search using the SD-433 and UMD arrays [10]. These events were acquired between December 2020 and March 2022 and correspond to approximately 10% of the complete high-quality dataset.

For photon search applications, a candidate selection cut must be defined. Following standard practice, we used the median of the photon score distributions in each energy bin to set the candidate threshold. A linear model is used to describe the energy dependence. Figure 5 exhibits the scores from all three classifiers as a function of the photon energy. Simulated photons, protons, and iron nuclei are displayed for comparison, along with the burnt sample (black stars).

All three scores yield distributions that clearly separate photons from hadronic backgrounds, with the SD–UMD score providing the cleanest separation. None of the events from the burnt dataset cross the candidate cut in any of the three scores. The absence of candidates is consistent with a fully hadronic population and aligns with the findings reported in [10].
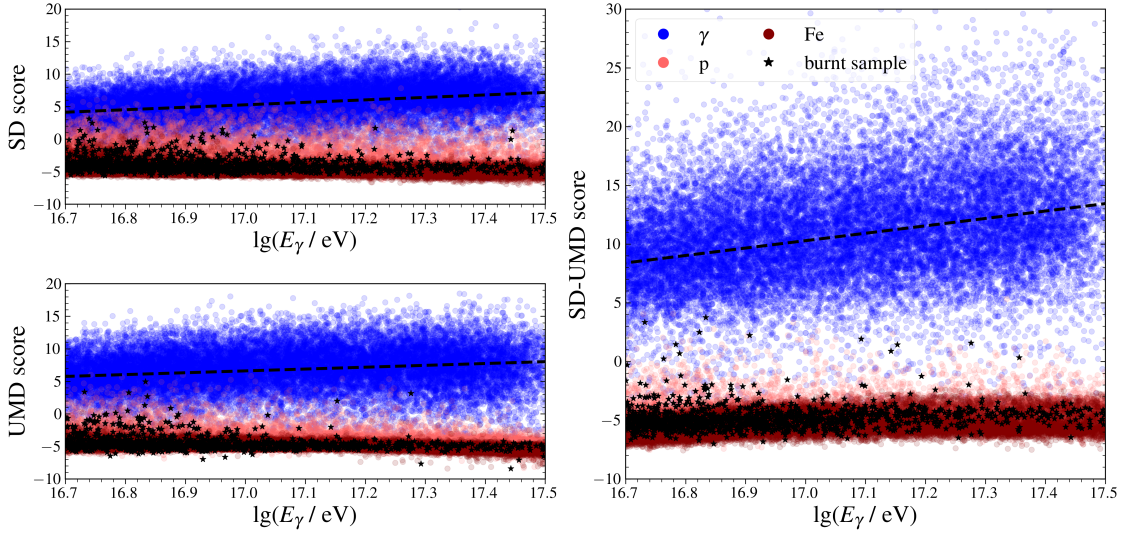

Figure 5: Classification scores from the SD (top left), UMD (bottom left), and SD–UMD (right) heads as a function of photon energy. Simulated photons, protons, and iron nuclei are shown, along with burnt sample events (black stars). Dashed lines indicate candidate selection thresholds based on the photon medians.

6. Summary and outlook

We have developed a graph-based neural network to discriminate between photon and hadron primaries in extensive air showers measured at the Pierre Auger Observatory. By encoding the spatio-temporal information of the SD-433 and the UMD into a unified graph representation, and

processing these through a multi-path architecture with graph attention layers, the model achieves strong photon–hadron separation across the energy range 50–300 PeV. Using the SD-UMD score of the GNN we achieve a background contamination level of at least 10^{-5} for a signal efficiency of 0.5 in realistic scenarios where one or more UMD stations are not operative.

The model was trained and validated on a realistic simulation data set that includes detector inefficiencies and reconstruction with photon priors. Its performance was assessed on both test simulations and a previously burnt subset of data, showing compatibility with hadronic expectations and validating the application of deep learning techniques to data. Conservative background contamination estimates were derived through exponential tail fits with bootstrap uncertainties, which underscore the current limitation posed by the low statistics in the photon-like tail of proton events.

Deep learning methods now complement traditional photon search techniques at the Pierre Auger Observatory. As with previous approaches, the main limitation remains to be the exposure, due to the extremely low expected photon flux. With accumulating statistics, future efforts should prioritize more accurate background modeling and the enhancement of the sensitivity to photon primaries. Whether through a discovery or the setting of tighter upper limits, these searches will increasingly constrain cosmogenic photon fluxes and models involving SHDM particles. In particular, the growing exposure of the SD-433 array and UMD will allow us to test the hypothesis of a diffuse photon flux originating from pp interactions in the Galactic halo [17], as well as predictions from two distinct SHDM decay scenarios [18, 19].

References

[1] A. Bobrikova et al., PoS **395** (2021) 449.

[2] C. Bérat et al., Astrophys. J. **929** (2022) 55.

[3] B. Sarkar et al., ICRC (Beijing) **2** (2011) 198.

[4] P. Abreu et al. [Pierre Auger Collaboration], Phys. Rev. D **107** (2023) 042002.

[5] A. Aab et al. [Pierre Auger Collaboration], arXiv:1604.03637.

[6] J. de Jesus et al. [Pierre Auger Collaboration], PoS **444** (2023) 267.

[7] C. Pérez Bertolli et al. [Pierre Auger Collaboration], PoS(EPS-HEP2023) **449** (2024) 535.

[8] M. Scornavacche et al. [Pierre Auger Collaboration], EPJ Web Conf. **283** (2023) 06012.

[9] A. Aab et al. [Pierre Auger Collaboration], JINST **11** (2016) 2012

[10] A. Abdul Halim et al. [Pierre Auger Collaboration], JCAP **2025** (05) 061.

[11] D. Heck et al., Forschungszentrum Karlsruhe Report FZKA **6019** (1998) .

[12] T. Pierog et al., Phys. Rev. C **92** (2015) 034906.

[13] S. Argiro et al., Nucl. Instrum. Meth. A **580** (2007) 1485-1496.

[14] G. Brichetto et al. [Pierre Auger Collaboration],PoS(ICRC2023) **444** (2023) 398.

[15] E. Rodriguez et al. [Pierre Auger Collaboration], PoS(UHECR2024) **484** (2025) 111.

[16] S. Brody et al., arXiv:2105.14491.

[17] O. E. Kalashev and S. V. Troitsky, JETP Lett. **100** (2014) 865.

[18] O. E. Kalashev and M. Yu. Kuznetsov, Phys. Rev. D **94** (2016) 063535.

[19] M. Kachelriess, O. E. Kalashev, and M. Yu. Kuznetsov, Phys. Rev. D **98** (2018) 083016.

The Pierre Auger Collaboration
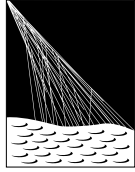
A. Abdul Halim[13], P. Abreu[70], M. Aglietta[53,51], I. Allekotte[1], K. Almeida Cheminant[78,77], A. Almela[7,12], R. Aloisio[44,45], J. Alvarez-Muñiz[76], A. Ambrosone[44], J. Ammerman Yebra[76], G.A. Anastasi[57,46], L. Anchordoqui[83], B. Andrada[7], L. Andrade Dourado[44,45], S. Andringa[70], L. Apollonio[58,48], C. Aramo[49], E. Arnone[62,51], J.C. Arteaga Velázquez[66], P. Assis[70], G. Avila[11], E. Avocone[56,45], A. Bakalova[31], F. Barbato[44,45], A. Bartz Mocellin[82], J.A. Bellido[13], C. Berat[35], M.E. Bertaina[62,51], M. Bianciotto[62,51], P.L. Biermann[a], V. Binet[5], K. Bismark[38,7], T. Bister[77,78], J. Biteau[36,i], J. Blazek[31], J. Blümer[40], M. Boháčová[31], D. Boncioli[56,45], C. Bonifazi[8], L. Bonneau Arbeletche[22], N. Borodai[68], J. Brack[f], P.G. Brichetto Orchera[7,40], F.L. Briechle[41], A. Bueno[75], S. Buitink[15], M. Buscemi[46,57], M. Büsken[38,7], A. Bwembya[77,78], K.S. Caballero-Mora[65], S. Cabana-Freire[76], L. Caccianiga[58,48], F. Campuzano[6], J. Caraça-Valente[82], R. Caruso[57,46], A. Castellina[53,51], F. Catalani[19], G. Cataldi[47], L. Cazon[76], M. Cerda[10], B. Čermáková[40], A. Cermenati[44,45], J.A. Chinellato[22], J. Chudoba[31], L. Chytka[32], R.W. Clay[13], A.C. Cobos Cerutti[6], R. Colalillo[59,49], R. Conceição[70], G. Consolati[48,54], M. Conte[55,47], F. Convenga[44,45], D. Correia dos Santos[27], P.J. Costa[70], C.E. Covault[81], M. Cristinziani[43], C.S. Cruz Sanchez[3], S. Dasso[4,2], K. Daumiller[40], B.R. Dawson[13], R.M. de Almeida[27], E.-T. de Boone[43], B. de Errico[27], J. de Jesús[7], S.J. de Jong[77,78], J.R.T. de Mello Neto[27], I. De Mitri[44,45], J. de Oliveira[18], D. de Oliveira Franco[42], F. de Palma[55,47], V. de Souza[20], E. De Vito[55,47], A. Del Popolo[57,46], O. Deligny[33], N. Denner[31], L. Deval[53,51], A. di Matteo[51], C. Dobrigkeit[22], J.C. D'Olivo[67], L.M. Domingues Mendes[16,70], Q. Dorosti[43], J.C. dos Anjos[16], R.C. dos Anjos[26], J. Ebr[31], F. Ellwanger[40], R. Engel[38,40], I. Epicoco[55,47], M. Erdmann[41], A. Etchegoyen[7,12], C. Evoli[44,45], H. Falcke[77,79,78], G. Farrar[85], A.C. Fauth[22], T. Fehler[43], F. Feldbusch[39], A. Fernandes[70], M. Fernandez[14], B. Fick[84], J.M. Figueira[7], P. Filip[38,7], A. Filipčič[74,73], T. Fitoussi[40], B. Flaggs[87], T. Fodran[77], A. Franco[47], M. Freitas[70], T. Fujii[86,h], A. Fuster[7,12], C. Galea[77], B. García[6], C. Gaudu[37], P.L. Ghia[33], U. Giaccari[47], F. Gobbi[10], F. Gollan[7], G. Golup[1], M. Gómez Berisso[1], P.F. Gómez Vitale[11], J.P. Gongora[11], J.M. González[1], N. González[7], D. Góra[68], A. Gorgi[53,51], M. Gottowik[40], F. Guarino[59,49], G.P. Guedes[23], L. Gülzow[40], S. Hahn[38], P. Hamal[31], M.R. Hampel[7], P. Hansen[3], V.M. Harvey[13], A. Haungs[40], T. Hebbeker[41], C. Hojvat[d], J.R. Hörandel[77,78], P. Horvath[32], M. Hrabovský[32], T. Huege[40,15], A. Insolia[57,46], P.G. Isar[72], M. Ismaiel[77,78], P. Janecek[31], V. Jilek[31], K.-H. Kampert[37], B. Keilhauer[40], A. Khakurdikar[77], V.V. Kizakke Covilakam[7,40], H.O. Klages[40], M. Kleifges[39], J. Köhler[40], F. Krieger[41], M. Kubatova[31], N. Kunka[39], B.L. Lago[17], N. Langner[41], N. Leal[7], M.A. Leigui de Oliveira[25], Y. Lema-Capeans[76], A. Letessier-Selvon[34], I. Lhenry-Yvon[33], L. Lopes[70], J.P. Lundquist[73], M. Mallamaci[60,46], D. Mandat[31], P. Mantsch[d], F.M. Mariani[58,48], A.G. Mariazzi[3], I.C. Mariş[14], G. Marsella[60,46], D. Martello[55,47], S. Martinelli[40,7], M.A. Martins[76], H.-J. Mathes[40], J. Matthews[g], G. Matthiae[61,50], E. Mayotte[82], S. Mayotte[82], P.O. Mazur[d], G. Medina-Tanco[67], J. Meinert[37], D. Melo[7], A. Menshikov[39], C. Merx[40], S. Michal[31], M.I. Micheletti[5], L. Miramonti[58,48], M. Mogarkar[68], S. Mollerach[1], F. Montanet[35], L. Morejon[37], K. Mulrey[77,78], R. Mussa[51], W.M. Namasaka[37], S. Negi[31], L. Nellen[67], K. Nguyen[84], G. Nicora[9], M. Niechciol[43], D. Nitz[84], D. Nosek[30], A. Novikov[87], V. Novotny[30], L. Nožka[32], A. Nucita[55,47], L.A. Núñez[29], J. Ochoa[7,40], C. Oliveira[20], L. Östman[31], M. Palatka[31], J. Pallotta[9], S. Panja[31], G. Parente[76], T. Paulsen[37], J. Pawlowsky[37], M. Pech[31], J. Pękala[68], R. Pelayo[64], V. Pelgrims[14], L.A.S. Pereira[24], E.E. Pereira Martins[38,7], C. Pérez Bertolli[7,40], L. Perrone[55,47], S. Petrera[44,45], C. Petrucci[56], T. Pierog[40], M. Pimenta[70], M. Platino[7], B. Pont[77], M. Pourmohammad Shahvar[60,46], P. Privitera[86], C. Priyadarshi[68], M. Prouza[31], K. Pytel[69], S. Querchfeld[37], J. Rautenberg[37], D. Ravignani[7], J.V. Reginatto Akim[22], A. Reuzki[41], J. Ridky[31], F. Riehn[76,j], M. Risse[43], V. Rizi[56,45], E. Rodriguez[7,40], G. Rodriguez Fernandez[50], J. Rodriguez Rojo[11], S. Rossoni[42], M. Roth[40], E. Roulet[1], A.C. Rovero[4], A. Saftoiu[71], M. Saharan[77], F. Salamida[56,45], H. Salazar[63], G. Salina[50], P. Sampathkumar[40], N. San Martin[82], J.D. Sanabria Gomez[29], F. Sánchez[7], E.M. Santos[21], E. Santos[31], F. Sarazin[82], R. Sarmento[70], R. Sato[11], P. Savina[44,45], V. Scherini[55,47], H. Schieler[40], M. Schimassek[33], M. Schimp[37], D. Schmidt[40], O. Scholten[15,b], H. Schoorlemmer[77,78], P. Schovánek[31], F.G. Schröder[87,40], J. Schulte[41], T. Schulz[31], S.J. Sciutto[3], M. Scornavacche[7], A. Sedoski[7], A. Segreto[52,46], S. Sehgal[37], S.U. Shivashankara[73], G. Sigl[42], K. Simkova[15,14], F. Simon[39], R. Šmída[86], P. Sommers[e], R. Squartini[10], M. Stadelmaier[40,48,58], S. Stanič[73], J. Stasielak[68], P. Stassi[35], S. Strähnz[38], M. Straub[41], T. Suomijärvi[36], A.D. Supanitsky[7], Z. Svozilikova[31], K. Syrokvas[30], Z. Szadkowski[69], F. Tairli[13], M. Tambone[59,49], A. Tapia[28], C. Taricco[62,51], C. Timmermans[78,77], O. Tkachenko[31], P. Tobiska[31], C.J. Todero Peixoto[19], B. Tomé[70], A. Travaini[10], P. Travnicek[31], M. Tueros[3], M. Unger[40], R. Uzeiroska[37], L. Vaclavek[32], M. Vacula[32], I. Vaiman[44,45], J.F. Valdés Galicia[67], L. Valore[59,49], P. van Dillen[77,78], E. Varela[63], V. Vašíčková[37], A. Vásquez-Ramírez[29], D. Veberič[40], I.D. Vergara Quispe[3], S. Verpoest[87], V. Verzi[50], J. Vicha[31], J. Vink[80], S. Vorobiov[73], J.B. Vuta[31], C. Watanabe[27], A.A. Watson[c], A. Weindl[40], M. Weitz[37], L. Wiencke[82], H. Wilczyński[68], B. Wundheiler[7], B. Yue[37], A. Yushkov[31], E. Zas[76], D. Zavrtanik[73,74], M. Zavrtanik[74,73]

[1] Centro Atómico Bariloche and Instituto Balseiro (CNEA-UNCuyo-CONICET), San Carlos de Bariloche, Argentina

[2] Departamento de Física and Departamento de Ciencias de la Atmósfera y los Océanos, FCEyN, Universidad de Buenos Aires and CONICET, Buenos Aires, Argentina

[3] IFLP, Universidad Nacional de La Plata and CONICET, La Plata, Argentina

[4] Instituto de Astronomía y Física del Espacio (IAFE, CONICET-UBA), Buenos Aires, Argentina

[5] Instituto de Física de Rosario (IFIR) – CONICET/U.N.R. and Facultad de Ciencias Bioquímicas y Farmacéuticas U.N.R., Rosario, Argentina

[6] Instituto de Tecnologías en Detección y Astropartículas (CNEA, CONICET, UNSAM), and Universidad Tecnológica Nacional – Facultad Regional Mendoza (CONICET/CNEA), Mendoza, Argentina

[7] Instituto de Tecnologías en Detección y Astropartículas (CNEA, CONICET, UNSAM), Buenos Aires, Argentina

[8] International Center of Advanced Studies and Instituto de Ciencias Físicas, ECyT-UNSAM and CONICET, Campus Miguelete – San Martín, Buenos Aires, Argentina

[9] Laboratorio Atmósfera – Departamento de Investigaciones en Láseres y sus Aplicaciones – UNIDEF (CITEDEF-CONICET), Argentina

[10] Observatorio Pierre Auger, Malargüe, Argentina

[11] Observatorio Pierre Auger and Comisión Nacional de Energía Atómica, Malargüe, Argentina

[12] Universidad Tecnológica Nacional – Facultad Regional Buenos Aires, Buenos Aires, Argentina

[13] University of Adelaide, Adelaide, S.A., Australia

[14] Université Libre de Bruxelles (ULB), Brussels, Belgium

[15] Vrije Universiteit Brussels, Brussels, Belgium

[16] Centro Brasileiro de Pesquisas Fisicas, Rio de Janeiro, RJ, Brazil

[17] Centro Federal de Educação Tecnológica Celso Suckow da Fonseca, Petropolis, Brazil

[18] Instituto Federal de Educação, Ciência e Tecnologia do Rio de Janeiro (IFRJ), Brazil

[19] Universidade de São Paulo, Escola de Engenharia de Lorena, Lorena, SP, Brazil

[20] Universidade de São Paulo, Instituto de Física de São Carlos, São Carlos, SP, Brazil

[21] Universidade de São Paulo, Instituto de Física, São Paulo, SP, Brazil

[22] Universidade Estadual de Campinas (UNICAMP), IFGW, Campinas, SP, Brazil

[23] Universidade Estadual de Feira de Santana, Feira de Santana, Brazil

[24] Universidade Federal de Campina Grande, Centro de Ciencias e Tecnologia, Campina Grande, Brazil

[25] Universidade Federal do ABC, Santo André, SP, Brazil

[26] Universidade Federal do Paraná, Setor Palotina, Palotina, Brazil

[27] Universidade Federal do Rio de Janeiro, Instituto de Física, Rio de Janeiro, RJ, Brazil

[28] Universidad de Medellín, Medellín, Colombia

[29] Universidad Industrial de Santander, Bucaramanga, Colombia

[30] Charles University, Faculty of Mathematics and Physics, Institute of Particle and Nuclear Physics, Prague, Czech Republic

[31] Institute of Physics of the Czech Academy of Sciences, Prague, Czech Republic

[32] Palacky University, Olomouc, Czech Republic

[33] CNRS/IN2P3, IJCLab, Université Paris-Saclay, Orsay, France

[34] Laboratoire de Physique Nucléaire et de Hautes Energies (LPNHE), Sorbonne Université, Université de Paris, CNRS-IN2P3, Paris, France

[35] Univ. Grenoble Alpes, CNRS, Grenoble Institute of Engineering Univ. Grenoble Alpes, LPSC-IN2P3, 38000 Grenoble, France

[36] Université Paris-Saclay, CNRS/IN2P3, IJCLab, Orsay, France

[37] Bergische Universität Wuppertal, Department of Physics, Wuppertal, Germany

[38] Karlsruhe Institute of Technology (KIT), Institute for Experimental Particle Physics, Karlsruhe, Germany

[39] Karlsruhe Institute of Technology (KIT), Institut für Prozessdatenverarbeitung und Elektronik, Karlsruhe, Germany

[40] Karlsruhe Institute of Technology (KIT), Institute for Astroparticle Physics, Karlsruhe, Germany

[41] RWTH Aachen University, III. Physikalisches Institut A, Aachen, Germany

[42] Universität Hamburg, II. Institut für Theoretische Physik, Hamburg, Germany

[43] Universität Siegen, Department Physik – Experimentelle Teilchenphysik, Siegen, Germany

[44] Gran Sasso Science Institute, L'Aquila, Italy

[45] INFN Laboratori Nazionali del Gran Sasso, Assergi (L'Aquila), Italy

[46] INFN, Sezione di Catania, Catania, Italy

[47] INFN, Sezione di Lecce, Lecce, Italy

[48] INFN, Sezione di Milano, Milano, Italy

[49] INFN, Sezione di Napoli, Napoli, Italy

[50] INFN, Sezione di Roma "Tor Vergata", Roma, Italy

[51] INFN, Sezione di Torino, Torino, Italy

[52] Istituto di Astrofisica Spaziale e Fisica Cosmica di Palermo (INAF), Palermo, Italy

[53] Osservatorio Astrofisico di Torino (INAF), Torino, Italy

[54] Politecnico di Milano, Dipartimento di Scienze e Tecnologie Aerospaziali , Milano, Italy

[55] Università del Salento, Dipartimento di Matematica e Fisica "E. De Giorgi", Lecce, Italy

[56] Università dell'Aquila, Dipartimento di Scienze Fisiche e Chimiche, L'Aquila, Italy

[57] Università di Catania, Dipartimento di Fisica e Astronomia "Ettore Majorana", Catania, Italy

[58] Università di Milano, Dipartimento di Fisica, Milano, Italy

[59] Università di Napoli "Federico II", Dipartimento di Fisica "Ettore Pancini", Napoli, Italy

[60] Università di Palermo, Dipartimento di Fisica e Chimica "E. Segrè", Palermo, Italy

[61] Università di Roma "Tor Vergata", Dipartimento di Fisica, Roma, Italy

[62] Università Torino, Dipartimento di Fisica, Torino, Italy

[63] Benemérita Universidad Autónoma de Puebla, Puebla, México

[64] Unidad Profesional Interdisciplinaria en Ingeniería y Tecnologías Avanzadas del Instituto Politécnico Nacional (UPIITA-IPN), México, D.F., México

[65] Universidad Autónoma de Chiapas, Tuxtla Gutiérrez, Chiapas, México

[66] Universidad Michoacana de San Nicolás de Hidalgo, Morelia, Michoacán, México

[67] Universidad Nacional Autónoma de México, México, D.F., México

[68] Institute of Nuclear Physics PAN, Krakow, Poland

[69] University of Łódź, Faculty of High-Energy Astrophysics,Łódź, Poland

[70] Laboratório de Instrumentação e Física Experimental de Partículas – LIP and Instituto Superior Técnico – IST, Universidade de Lisboa – UL, Lisboa, Portugal

[71] "Horia Hulubei" National Institute for Physics and Nuclear Engineering, Bucharest-Magurele, Romania

[72] Institute of Space Science, Bucharest-Magurele, Romania

[73] Center for Astrophysics and Cosmology (CAC), University of Nova Gorica, Nova Gorica, Slovenia

[74] Experimental Particle Physics Department, J. Stefan Institute, Ljubljana, Slovenia

[75] Universidad de Granada and C.A.F.P.E., Granada, Spain

[76] Instituto Galego de Física de Altas Enerxías (IGFAE), Universidade de Santiago de Compostela, Santiago de Compostela, Spain

[77] IMAPP, Radboud University Nijmegen, Nijmegen, The Netherlands

[78] Nationaal Instituut voor Kernfysica en Hoge Energie Fysica (NIKHEF), Science Park, Amsterdam, The Netherlands

[79] Stichting Astronomisch Onderzoek in Nederland (ASTRON), Dwingeloo, The Netherlands

[80] Universiteit van Amsterdam, Faculty of Science, Amsterdam, The Netherlands

[81] Case Western Reserve University, Cleveland, OH, USA

[82] Colorado School of Mines, Golden, CO, USA

[83] Department of Physics and Astronomy, Lehman College, City University of New York, Bronx, NY, USA

[84] Michigan Technological University, Houghton, MI, USA

[85] New York University, New York, NY, USA

[86] University of Chicago, Enrico Fermi Institute, Chicago, IL, USA

[87] University of Delaware, Department of Physics and Astronomy, Bartol Research Institute, Newark, DE, USA

———

[a] Max-Planck-Institut für Radioastronomie, Bonn, Germany

[b] also at Kapteyn Institute, University of Groningen, Groningen, The Netherlands

[c] School of Physics and Astronomy, University of Leeds, Leeds, United Kingdom

[d] Fermi National Accelerator Laboratory, Fermilab, Batavia, IL, USA

[e] Pennsylvania State University, University Park, PA, USA

[f] Colorado State University, Fort Collins, CO, USA

[g] Louisiana State University, Baton Rouge, LA, USA

[h] now at Graduate School of Science, Osaka Metropolitan University, Osaka, Japan

[i] Institut universitaire de France (IUF), France

[j] now at Technische Universität Dortmund and Ruhr-Universität Bochum, Dortmund and Bochum, Germany

Acknowledgments